

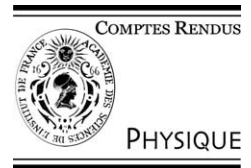


ELSEVIER

Available online at www.sciencedirect.com

SCIENCE @ DIRECT®

C. R. Physique 4 (2003) 649–661



Semiconductor lasers/Lasers semiconducteurs

High-brightness diode lasers

Hans Wenzel *, Bernd Sumpf, Götz Erbert

Ferdinand-Braun-Institut für Höchstfrequenztechnik, Albert-Einstein-Strasse 11, 12489 Berlin, Germany

Received 10 March 2003; accepted 11 March 2003

Presented by Guy Laval

Abstract

The basic concepts and some modelling aspects of high-brightness semiconductor lasers are reviewed. The technology of lasers with a tapered gain-region is described. They provide the highest brightness of a semiconductor source with continuous wave emission in the visible and near infrared spectral range. Experimental results are presented for tapered lasers emitting at 735 nm and 808 nm. Output powers of 3 W were achieved in nearly diffraction limited beams. **To cite this article: H. Wenzel et al., C. R. Physique 4 (2003).**

© 2003 Académie des sciences. Published by Éditions scientifiques et médicales Elsevier SAS. All rights reserved.

Résumé

Diodes laser de forte luminance. Les concepts de base et certains aspects de la modélisation des lasers semiconducteurs de haute luminance sont passés en revue. La technologie des lasers comportant une section amplificatrice évasée est décrite. Ils constituent les sources semiconductrices émettant en continu ayant la plus forte luminance dans le domaine spectral visible et proche infrarouge. Des résultats expérimentaux sont présentés pour des lasers évasés émettant à 735 nm et à 808 nm. Des puissances de 3 W ont été obtenues avec des faisceaux presque limités par la diffraction. **Pour citer cet article : H. Wenzel et al., C. R. Physique 4 (2003).**

© 2003 Académie des sciences. Published by Éditions scientifiques et médicales Elsevier SAS. All rights reserved.

Keywords: Semiconductor lasers; High brightness; High power; Beam quality; Tapered lasers; Modelling

Mots-clés : Lasers semiconducteurs ; Forte luminance ; Forte puissance ; Qualité de faisceau ; Lasers évasés ; Modélisation

1. Introduction

High-power coherent optical beams are needed for a number of applications such as for fibre and space telecommunication [1], nonlinear optical frequency conversion [2], medical treatments [3] and material processing [4]. Although high-power beams can be generated by gas and solid state lasers, semiconductor lasers offer the advantages of high efficiency, improved reliability, reduced cost, small size and ease of handling. However, an increase of the output power above 1 W either rapidly deteriorates the beam quality or results in reliability problems, due to the small spot size of standard semiconductor lasers. Nevertheless, beam quality can be improved significantly with an appropriate device design, resulting in a high brightness laser diode. During the last years, a number of solutions have been investigated, including master-oscillator power-amplifier (MOPA) configurations, tapered gain-region lasers and angled-grating distributed feedback (α -DFB) lasers. Among these structures, tapered lasers have received the greatest attention because of the simplicity of their operational principles and fabrication processes.

* Corresponding author.

E-mail address: wenzel@fbh-berlin.de (H. Wenzel).

In this review, we begin by presenting some basic concepts used to increase the brightness of semiconductor lasers. In Section 3, we give an overview of different modelling tools that can be used for the computer-aided design of high-brightness lasers. In Section 4, we describe their fabrication and in Section 5 we present experimental results from tapered lasers emitting at 735 nm and 808 nm.

2. Basic concepts

We start with some definitions. The brightness of a light source is defined as the power P emitted per unit surface area A per unit solid angle Ω [5],

$$B = \frac{P}{A\Omega}. \tag{1}$$

Another important figure of merit is the so-called beam quality factor or beam propagation ratio [6]

$$M^2 = \frac{\pi \Theta w}{\lambda} \geq 1, \tag{2}$$

where Θ is the divergence angle and w the beam width at the waist. This factor specifies how much the beam divergence exceeds that of a Gaussian beam, so that M^2 is sometimes called the times-diffraction-limit factor. There are several methods to determine Θ and w . One method utilizes the corresponding angle and position, respectively, where the intensities of the far field and in the beam waist drop to $1/e^2$ of their maximum values. Another method is based on the second moments of the field profiles [7]. From an application point of view, we prefer the first method to determine M^2 because the weak side lobes in the near and far fields outside of the $1/e^2$ widths are often suppressed by spatial filtering. It is worth noting that some people use the full width at half maximum (FWHM) values and that this definition gives too optimistic values for M^2 .

If we introduce $A = \pi w^2$ and $\Omega = \pi \Theta^2$ in Eq. (1) and take into account Eq. (2) we obtain

$$B = \frac{P}{M^4 \lambda^2}. \tag{3}$$

So far, all of the expressions above are only valid for circular beams. While high-power semiconductor lasers typically have elliptical beams, these expressions have to be properly modified. For example, the beam propagation ratio in the denominator of Eq. (3) has to be replaced by

$$M_{\text{eff}}^4 = M_x^2 M_y^2, \tag{4}$$

where M_x^2 and M_y^2 are the corresponding beam propagation ratios along the x and y directions (compare Fig. 1). For typical high-power semiconductor lasers the approximation $M_x^2 \approx 1$ is valid.

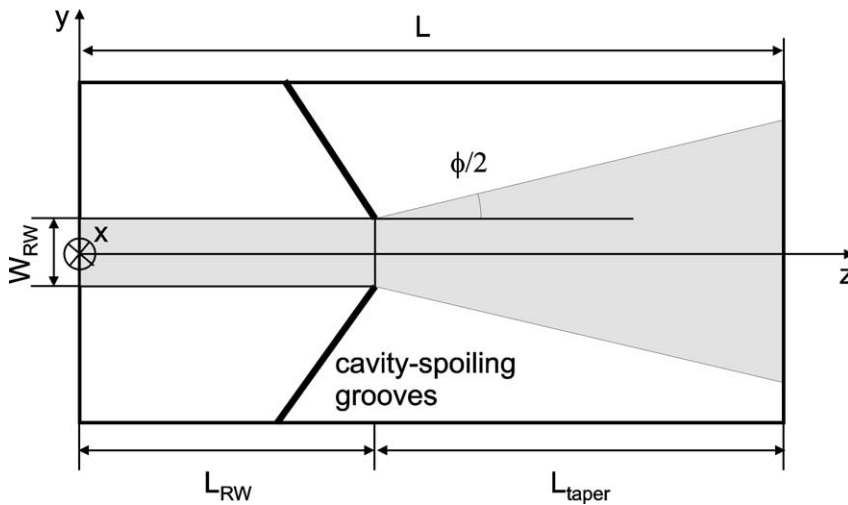


Fig. 1. Schematic top view of a tapered laser. The grey area corresponds to the p-contact region. The coordinate system used in the simulation is also sketched.

From Eq. (3), it follows immediately that the laser has to emit a high optical power in a nearly diffraction limited beam ($M^2 \approx 1$) in order to achieve high brightness. In diode lasers, the maximum possible CW power is often limited by the catastrophic optical mirror damage (COMD). From the definition of the internal power density at COMD, p_{COMD} , one can express the maximum CW power as [8]

$$P_{\text{max}} = \left(\frac{d}{\Gamma}\right)W \left(\frac{1-R}{1+R}\right)p_{\text{COMD}}, \quad (5)$$

where W is the lateral near field width and R the reflectivity of the output facet. The factor d/Γ is called ‘equivalent vertical spotsize’ and is a measure of the vertical near field width where d is thickness of the active layer and Γ the vertical optical confinement factor. From Eq. (5), it follows, that Γ and R must be reduced for high-power operation. However, they cannot be arbitrary reduced, because otherwise the laser performance deteriorates, resulting in a large threshold current, a low efficiency and a high temperature sensitivity.

The power density at COMD, p_{COMD} , is of the order of 10 MW/cm² and depends on the material system used (AlGaAs or InGaAsP), the epitaxial layer structure and intrinsic parameters. Although p_{COMD} can be increased by proper facet treatments, the most effective way to raise the maximum power is to increase W . However, increasing W immediately leads to difficulties in maintaining a single lateral mode so that M^2 rises up to values of 100 in single stripe broad-area emitters [9]. Hence, the basic task for making high-brightness diode lasers is the suppression of higher order lateral modes. There are different approaches to solve this problem. Here we will discuss only the most successful ones. For the other approaches we refer the readers to the review article of Walpole [5].

One approach exploits all-semiconductor master-oscillator power-amplifier (MOPA) configurations, where the relatively low optical output power of a spatial-single mode laser diode is injected into a semiconductor optical amplifier. The highest brightness has been achieved with so called flared or tapered gain-region amplifiers, whose width W increases linearly along the amplifying region. If the input aperture and the flared angle is designed correctly, the beam will diffract to fill the tapered gain region and will grow as it propagates towards the large output aperture. Since the tapered design uses a diverging beam, it is more stable with respect to non-linear distortions (e.g., filamentation) than a broad-stripe amplifier. In order to shift the lasing threshold of the amplifier to injection currents as high as possible, both facets have to be provided with anti-reflection coatings having reflection coefficients $R < 10^{-3}$.

The all-semiconductor MOPA can be realized in a hybrid configuration [10–12] or monolithically integrated [13–15]. The hybrid approach offers the advantage that the master-oscillator and the power-amplifier can be optimised separately, and that both can be optically well-isolated from each other. The disadvantage of the hybrid approach is the expensive mounting and alignment needed to fix both devices to each other.

The monolithically integrated MOPA is formed by integrating a narrow-stripe, single-spatial mode, index-guided distributed feedback (DFB) or distributed Bragg reflector (DBR) laser together with a gain-guided tapered amplifier. A buried Bragg grating is necessary because of the negligible reflectivity between the single-spatial mode waveguide and the tapered amplifier and the anti-reflection coated output facet. The disadvantage of the integration of the master-oscillator and the power amplifier on the same chip is that the active layers of both devices cannot be separately optimised. Furthermore, the devices exhibit a fairly complicated dynamic behaviour [16,17]. These non-linear instabilities are mainly caused by a residual output facet reflectivity. Thus, the monolithically integrated MOPA behaves like a laser with external feedback, which is known to show a large variety of dynamic phenomena [18].

If the Bragg grating formed in a monolithically integrated MOPA is partially or completely omitted and the output facet is provided with a finite, albeit small, reflectivity, we end up with a flared or tapered gain-region laser, compare Fig. 1 [19–27]. The tapered laser is an example of an unstable-cavity laser. The single-mode waveguide acts as a mode-filter because higher order lateral modes excited in the tapered region and propagating into the waveguide will dissipate there by both absorption and radiating into the radiation modes before they can propagate back into the tapered region. This mode-filtering effect can be enhanced by cavity-spoiling elements which deflect and scatter unwanted radiation away from the tapered region. They consist of grooves etched down through the active region and angled with respect both to the axis of symmetry of tapered structure and to the plane of the active layer.

The advantage of tapered lasers over monolithic MOPA configurations is the absence of the non-linear instabilities due to the double-cavity effects. Due to the absence of the buried Bragg gratings, formed within the structure, a tapered laser can be grown in one epitaxial run and is hence much easier to fabricate.

The main drawback of tapered amplifiers and lasers is the large astigmatism. Depending on the length of the tapered region, the beam waists for the lateral and vertical directions are located at very different positions. The output beam of an angled-grating (α -)DFB laser, where a tilted Bragg grating stabilizes the mode in both the longitudinal and lateral directions, lacks this strong astigmatism [28–32]. However, α -DFB lasers possess a lower efficiency and kinky light-current characteristics at higher output powers. Furthermore, their fabrication requires two epitaxial growth steps due the buried Bragg grating. Thus, the

tapered laser is currently the most promising candidate for a commercial exploitation as high-brightness semiconductor based light source.

3. Modelling

For the computer-aided design of diode lasers, a hierarchy of models can be used, starting from relatively simple ones running on a PC and extending to very complicated tools which require a super computer. For the simulation of light-current characteristics or field distributions, models which only simulate the stationary behaviour are usually sufficient. However, if one is interested in the dynamic behaviour or if non-linear instabilities emerge, the models must include the time t as an additional independent variable.

A prerequisite for any kind of simulation is the knowledge of the material-dependent parameters entering the models. For ternary and quaternary semiconductor compounds, these parameters and their wavelength and temperature dependencies are usually not well known. Often there are only a few experimental data available from measurements or first-principle calculations at selected compositions, wavelengths or temperatures. Hence, the parameters are mostly calculated by suitable interpolation formulas from the associated binary compounds. However, not all of the necessary parameters are even known for the binary compounds. There are several collections of parameters published in the literature, see, for example, [33–35] and the references therein.

Any design of a semiconductor laser starts with the modelling of the epitaxial layer structure. A one-dimensional optical mode solver is needed here in order to calculate the confinement factors and field distributions. In order to investigate the influence of the substrate in GaAs-based lasers, the optical solver should be able to treat complex valued dielectric function profiles [36]. Figs. 2 and 3 depict the results of such a calculation for the wavelength $\lambda = 808$ nm and a transverse-magnetic (TM) polarized mode. In Fig. 2, the equivalent vertical spotsize d/Γ of Eq. (5) is plotted versus the total width of the waveguide layer. From Fig. 2, it can be seen that if the Al content in the waveguide layer is reduced, the width must be correspondingly increased in order to keep $d/\Gamma \approx 1 \mu\text{m}$. This reduces not only the power density but also ensures a small vertical far field divergence (Fig. 3) which is useful for achieving good optical coupling efficiency. Additionally, the change of the effective index with carrier density is diminished [37], which reduces the formation of filaments through self-focusing of the optical field [39].

In order to optimise the active layer, which is usually composed of a single quantum well (QW) or of multiple quantum wells, one has to calculate the sub-bands and the local gain and refractive index spectra versus carrier density and temperature. This is usually done by solving the Schrödinger equation in the envelope approximation using the $\mathbf{k}\cdot\mathbf{p}$ method. Fig. 4 depicts

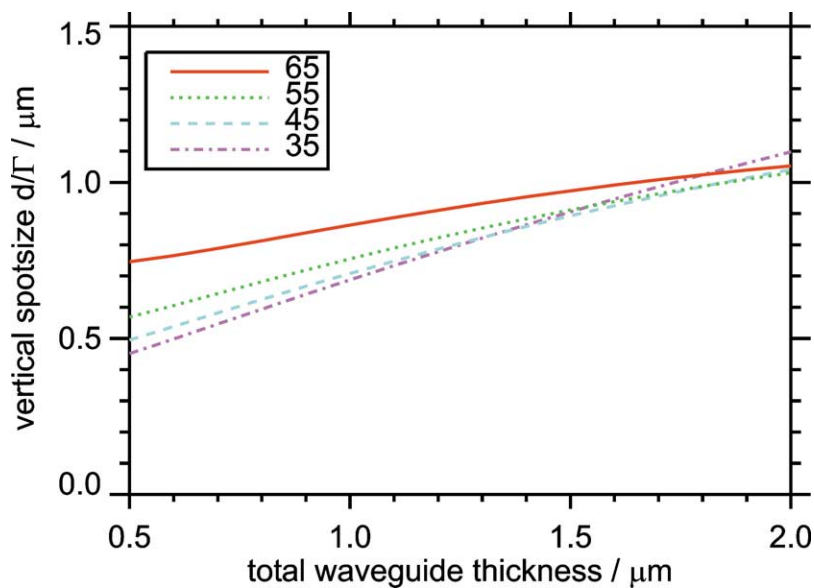


Fig. 2. Equivalent vertical spotsize versus the total waveguide width for different AlAs contents in % in the waveguide. The cladding layer consists of $\text{Al}_{0.7}\text{Ga}_{0.3}\text{As}$. The tensile-strained GaAsP QW has a thickness of $d = 14$ nm and is embedded in 10 nm AlGaAs linearly graded from the waveguide composition to $\text{Al}_{0.3}\text{Ga}_{0.7}\text{As}$. The wavelength is $\lambda = 808$ nm and the polarization is TM.

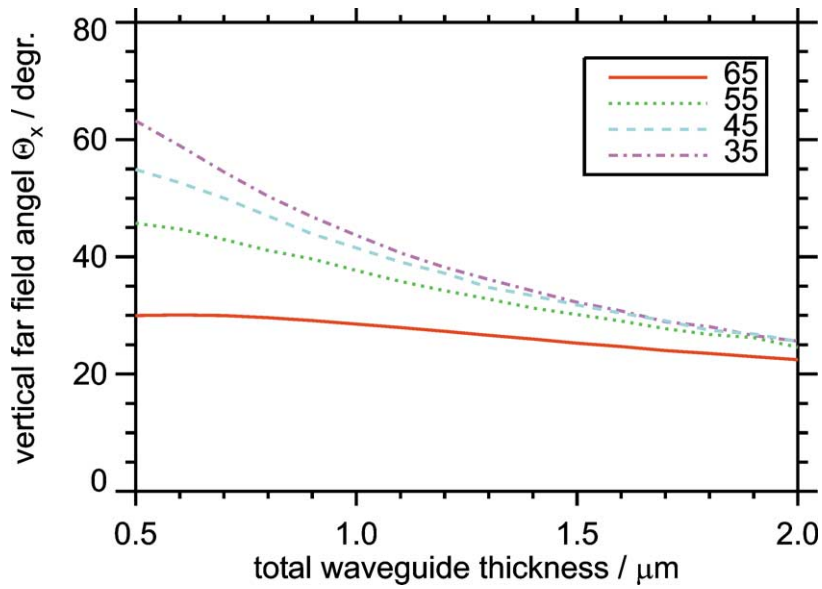


Fig. 3. Vertical far field angle (FWHM) versus the total wave guide width for different AlAs contents in % in the wave guide. Same parameters as in Fig. 2.

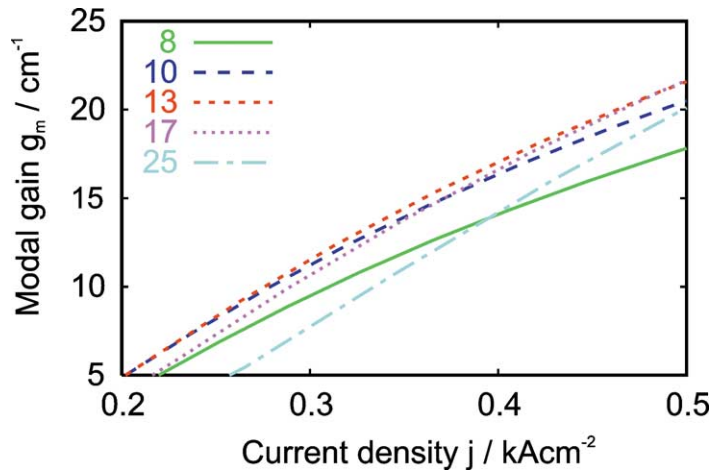


Fig. 4. Calculated TM modal peak gain versus current density for different GaAsP QW thicknesses in nm. The arsenic content has been chosen such that the transition wavelength between the electron subband edge and the light hole sub-band edge is approximately equal to 800 nm. The total wave guide thickness is 1 μm and consists of Al_{0.45}Ga_{0.55}As.

the result of such a simulation, which shows the impact of the thickness of a tensile strained GaAsP QW on the modal gain of the TM mode. The modal gain is the product of Γ and the local gain g . The calculations were performed using an eight-band $\mathbf{k}\cdot\mathbf{p}$ Hamiltonian and taking into account all possible transitions in QW as outlined in [37]. The current density consists of a radiative part consistently calculated with the gain, and a non-radiative part [38]. Although many-body effects are neglected, except for phenomenological corrections for the gain spectral broadening and for the band-gap renormalization, good agreement with measurements was achieved [40]. It can be concluded from Fig. 4 that for $\lambda = 808$ nm, a QW thickness between 10 and 17 nm is optimum, depending on the modal gain needed.

In order to calculate the current flow over pn and hetero junctions or the current spreading and carrier diffusion in laterally structured devices, drift-diffusion simulators must be employed [41]. For one-dimensional problems, a free simulator can be downloaded from the internet [42]. There are a number of commercial two-dimensional simulators available. They solve, self-consistently, in addition to the drift-diffusion equations, a heat-conduction equation and the equations for the optical field. The latter consist of a waveguide equation for the transverse mode distribution and a rate equation for the optical power. A simulation

of the temperature distribution alone (i.e., without a coupling to the electronic and optic equations) is often of little significance because of the improper consideration of the heat sources.

The above mentioned numerical simulators treat only the transverse plane assuming longitudinal homogeneity. The ‘treat power as a parameter’ (TPP) method [41,43] allows one to take into account at least the longitudinal spatial holeburning which is an important effect, for example, in high power lasers with a low-reflectivity output facet. A first three-dimensional simulation of tapered amplifiers and lasers has been reported in [44]. Within the EC-IST project ‘ULTRABRIGHT’, a sophisticated full

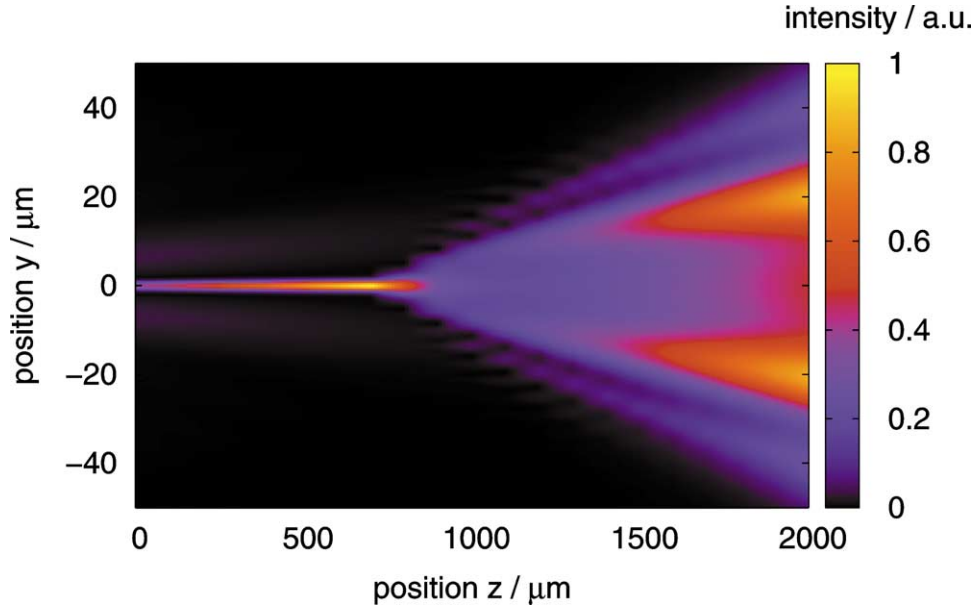


Fig. 5. Colour-scale plot of the intensity distribution of the forward propagating field in a tapered laser in the yz plane simulated with CONAN for the following parameters: $L = 2$ mm, $L_{RW} = 750$ μm , $W_{RW} = 2$ μm , $\varphi = 4^\circ$, $R_f = 1\%$. The output power is about $P = 1.7$ W. Only one half of the cavity ($y \geq 0$) was taken into account.

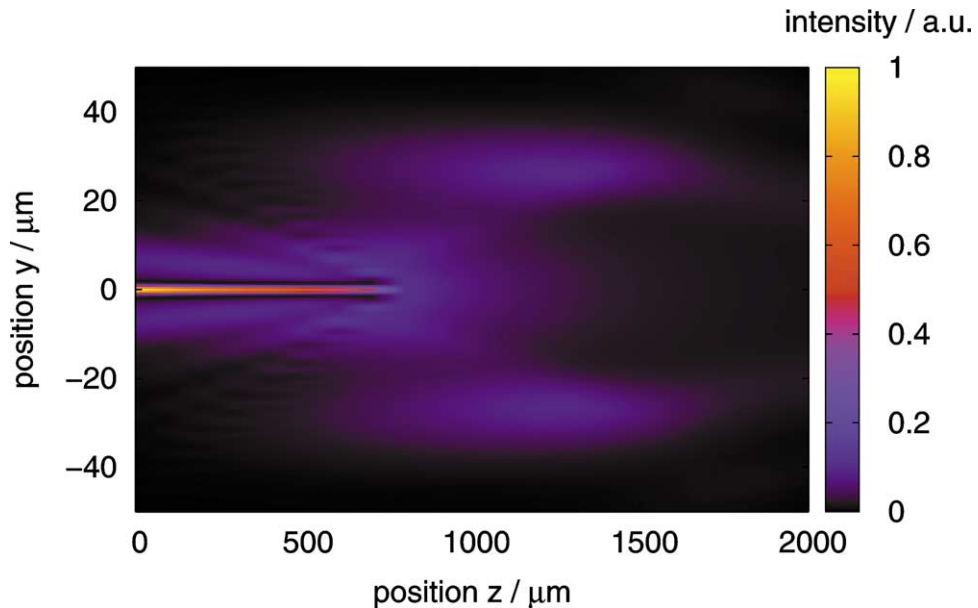


Fig. 6. Colour-scale plot of the intensity distribution of the backward propagating field in the yz plane simulated with CONAN. Same parameters as in Fig. 5.

three-dimensional simulator called ‘CONAN’ for longitudinal varying Fabry–Perot type of devices like tapered lasers has been developed by the University of Nottingham and Universidad Politécnica de Madrid. Instead of solving a rate equation for the optical power, a 3D wide-angle (WA) finite-difference (FD) beam propagation method (BPM) is used to solve the paraxial wave equation [45]. Figs. 5 and 6 depict the simulated forward and backward propagating optical fields, respectively, in a tapered laser at an output power $P = 1.7$ W. These results have been obtained with a preliminary version of CONAN, where the drift-diffusion and heat-conduction equations are solved two-dimensionally in slices along the longitudinal axis and the optical field is calculated with a 2D WA-FD-BPM using the effective-index approximation [46,47].

There are also a number of approximate two-dimensional numerical models specially developed for tapered lasers (for example, [48]) or α -DFB lasers [32], which solve the paraxial wave equation in the yz plane with a BPM and utilize greatly simplified equations for the carrier density and temperature distributions. Although the basic trends of a variation of geometrical and material parameters on the laser data can be predicted, a quantitative agreement with experiment is often difficult to achieve and the usefulness of such models for design purposes is limited.

As mentioned above, time-dependent models must be used if the generation of optical pulses or if non-linear instabilities such as self-sustained pulsations, switching phenomena or chaos are to be simulated. When numerically implementing such a model, one must take care that no instabilities are generated by the numerics and that the wavelength dependencies of the gain and the refractive index are properly translated into the time domain. One can distinguish between models that account only for the longitudinal coordinate z [17,49] or additionally for the lateral coordinate y [16] (compare Fig. 1). The most sophisticated model has been published by O. Hess and co-workers [50] which takes into account even the microscopic dynamics. However, the results are very difficult to interpret due to the complexity of the model.

In closing this Section, we would like to point to the internet site www.nusod.org where useful information about the numerical simulation of optoelectronic devices can be found.

4. Technology

In this Section, we describe a typical fabrication process for tapered lasers. A schematic three-dimensional picture of a processed laser is shown in Fig. 7. A straight ridge waveguide (RW) is usually used for the single-mode, index-guided region. Thus, the fabrication is based on a combination of well-established processing steps for RW and broad-area lasers, details of which can be found in the book [51]. In order to maximize the output power and to optimise the beam propagation ratio, the total cavity length L , the taper angle φ and the length L_{RW} can be varied (see Fig. 1).

The layer structures are grown on (001) exact-oriented GaAs substrates by a low-pressure metal-organic vapour phase epitaxy (MOVPE). This growth method has the advantage that phosphorous compounds like GaAsP which are used for the QW (see below) can be grown more easily than with molecular beam epitaxy (MBE). The precursors used for the growth of AlGaAs and GaAsP are TMGa, TMAI, AsH₃ and PH₃. DMZn and disilane are used for p- and n-doping, respectively. The purity of the sources is critical especially for shorter wavelength AlGaAs-based lasers. For example, in [52] it was shown that the incorporation of oxygen into the AlGaAs waveguides from a contaminated TMAI source is very critical for the performance of 735-nm emitting lasers, despite the use of an Al-free QW. The typical growth temperature of the laser structures is around

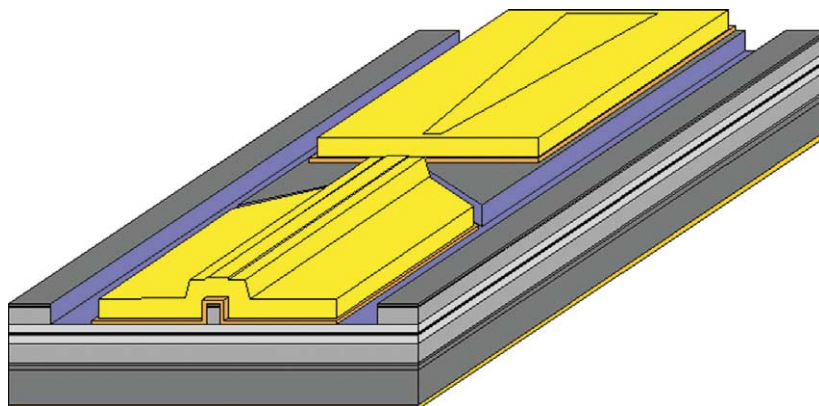


Fig. 7. Schematic three dimensional view of a tapered laser (not to scale). Grey: Epitaxial layer structure, dark yellow: n-contact metallisation, orange: p-contact metallisation, straw yellow: electroplated gold.

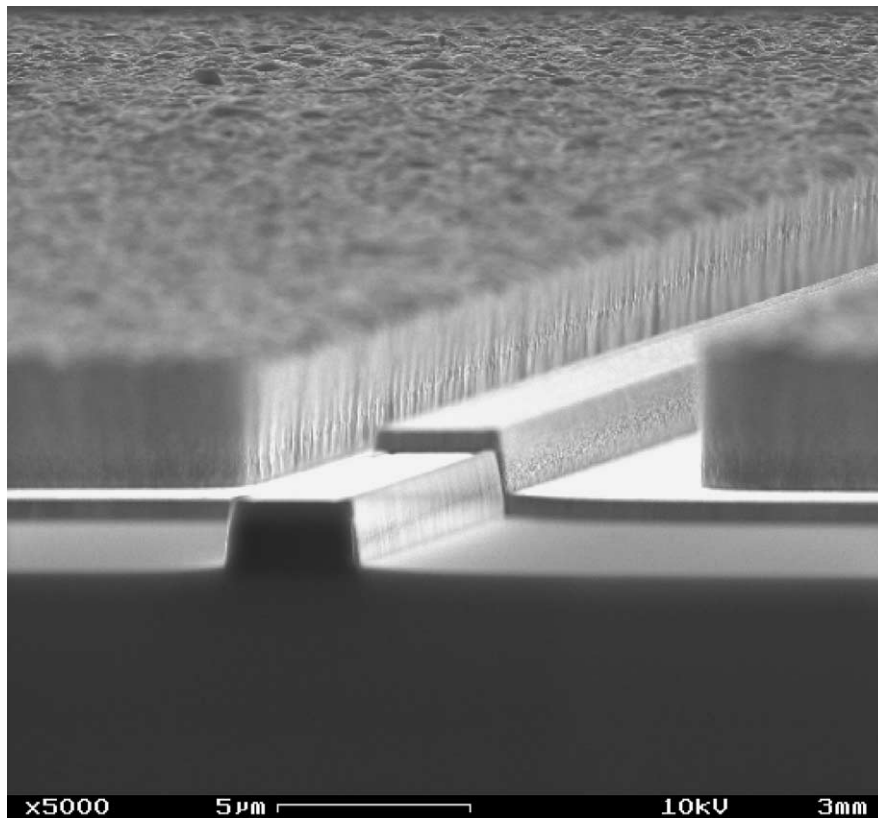


Fig. 8. SEM picture the rear facet and part of the RW region of a tapered laser. The dry etched ridge, the thin evaporated p-contact metallisation and the thick electroplated gold are visible. The thin (100 nm) insulating layer adjacent to the ridge cannot be seen clearly.

750 °C and the growth rate is about 3 μm/h. The thicknesses and compositions of the layers are determined by high-resolution X-ray diffraction and photo-luminescence spectroscopy.

The RW is fabricated by dry etching in our case, but wet-chemical etching in combination with an etch-stop layer could also be used. The ridge width W_{RW} is typically about 3 μm. The etch depth is around 1.5 μm, depending on the desired effective index step Δn_{eff} . Both W_{RW} and Δn_{eff} are critical parameters for ensuring single-mode behaviour and sufficient mode filtering properties. We should note, that the optimum taper angle φ depends on W_{RW} and Δn_{eff} . In Fig. 8, a scanning electron microscope (SEM) picture is shown of the rear facet of a tapered laser with the etched RW. Cavity spoiling elements, such as those discussed in Section 2, were not inserted. Although they enhance the mode filtering, they require additional processing steps and may be a source for degradation due to the need for deeply etched grooves.

The current spreading in the gain-guided tapered region can be reduced either by removing the p-GaAs contact layer by wet-chemical etching or by a low-energy He^+ implantation adjacent to the contact area. Additionally, a Si_3N_4 or Al_2O_3 layer is deposited for electrical isolation between the semiconductor surface and the p-contact metallisation outside of the RW and the tapered regions contact areas. The p-contact is realized with a standard Ti/Pt/Au layer system. A thick Au layer is electroplated to be able to mount the devices p-side down with AuSn solder [53].

After scribing and cleaving, the facets are coated using an ion-beam sputtering process to achieve the desired reflectivity. At the rear facet (RW region), the reflectivity is typically greater than 90%. The reflectivity R_f at the front (output) facet depends on the total cavity length L and can be optimised to obtain a large wall plug efficiency at the operating point and/or a good beam quality. In any case, the reflectivity is typically below 5% reaching values below 0.1% for longer cavity lengths $L > 2$ mm and high-gain materials. In tapered lasers, a low value of R_f also improves the beam quality by suppressing the optical pumping effect due to the reflected field.

The tapered lasers are mounted p-side down on T-cBN or CuW submounts using AuSn solder [53]. The thermal expansion coefficient (TEC) mismatch of both submount materials to GaAs is smaller than that of copper. This mounting scheme is more reliable than solutions based on In soldering directly on copper. T-cBN has a higher thermal conductivity than CuW, but a larger

TEC mismatch. Hence T-CBN is used for shorter (cavity length $L \leq 2$ mm) and CuW for longer devices. The subassemblies are typically mounted on standard copper heatsinks.

5. Experimental results

In this Section, typical results for tapered lasers emitting at $\lambda = 735$ nm and $\lambda = 808$ nm will be presented [25,26]. The wavelength range around 740 nm is especially interesting for the photodynamic therapy (PDT) [54], whereas high-brightness lasers emitting at 808 nm are used for pumping of solid-state lasers or for direct material processing [4]. Tapered lasers at these wavelengths are more challenging to fabricate than at wavelengths around 1000 nm because of smaller energetic barriers for electrons and holes and the larger Al-contents necessary [19,22–24,27].

At these wavelengths, the compound semiconductors AlInGaP or AlGaAs can be used for the bulk layers and InGaAsP or AlInGaAs for the active layer. We decided to use AlGaAs for both the waveguide and the cladding layers, because it is easy to grow and p-dope with zinc or carbon [55]. The QW consists of tensile-strained GaAsP, because of the nearly equal band offsets for electron and holes [38], the large differential gain and last, but not least, the absence of aluminium. Especially for 808 nm, the thickness and the composition of the QW have to be carefully optimised, compare Fig. 4. Due to the tensile strain, the lasing mode is TM polarized with the main component of the electric field vector perpendicular to the epitaxial layers.

The 735-nm emitting device consists of $\text{Al}_{0.7}\text{Ga}_{0.3}\text{As}$ cladding layers and a 1 μm thick $\text{Al}_{0.65}\text{Ga}_{0.35}\text{As}$ waveguide. The QW has a thickness of 9 nm. Broad-area devices made from this structure had an internal differential efficiency of $\eta_i = 0.8$, internal losses $\alpha_i < 1 \text{ cm}^{-1}$, a modal gain parameter $\Gamma g_0 = 20 \text{ cm}^{-1}$ and a transparency current density of $j_{tr} \leq 220 \text{ A/cm}^2$, assuming a logarithmic dependence of the modal gain on the current density. The 808-nm emitting device also consists of $\text{Al}_{0.7}\text{Ga}_{0.3}\text{As}$ cladding layers, but has a 2 μm thick $\text{Al}_{0.45}\text{Ga}_{0.55}\text{As}$ waveguide. The QW has a thickness of 17 nm (compare Fig. 4). At broad-area devices made from this structure the following figures of merit were measured: $\eta_i \geq 0.9$, $\alpha_i < 1 \text{ cm}^{-1}$, $\Gamma g_0 = 17 \text{ cm}^{-1}$, $j_{tr} \leq 150 \text{ A/cm}^2$. The full widths at half maximum (FWHM) of the vertical far field intensity profiles is 27° (732 nm) and 25° (808 nm), which agree quite well with the calculated values (see Fig. 3).

At first, we will present results for the 732-nm emitting devices with $L = 2.75$ mm, $\varphi = 6^\circ$, $L_{RW} = 1$ mm, $W_{RW} = 3 \mu\text{m}$, $R_f = 1\%$ and an effective-index step of $\Delta n_{\text{eff}} = 7 \times 10^{-3}$. The power-voltage-current characteristics are depicted in Fig. 9. The threshold current is below 0.8 A. The slope efficiency of above 0.9 W/A and maximum conversion efficiency of $\eta_c = 0.4$ are

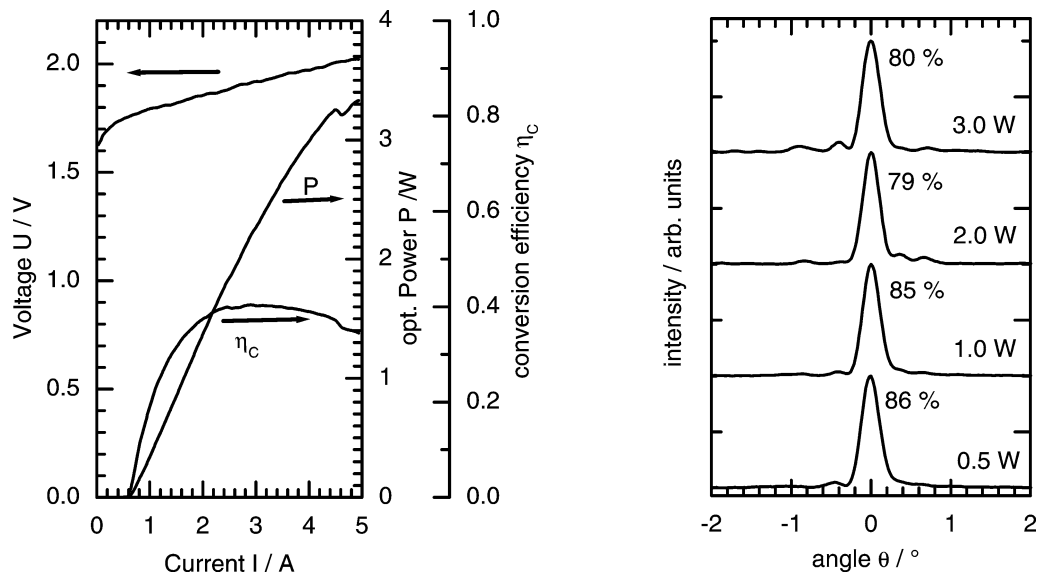


Fig. 9. CW voltage-power-current characteristics of a 732 nm tapered laser with the following parameters: $L = 2.75$ mm, $L_{RW} = 1$ mm, $W_{RW} = 3 \mu\text{m}$, $\varphi = 6^\circ$, $R_f = 1\%$. The heatsink temperature was $T = 25^\circ\text{C}$.

Fig. 10. Profile of the corrected lateral far field intensity at different output powers of a 732 nm tapered laser with the same parameters as in Fig. 9. The relative power in the central lobe is also indicated. The heatsink temperature was $T = 25^\circ\text{C}$.

only slightly smaller than those of corresponding broad area lasers, despite the additional radiation losses due to mode filtering. This is primarily due to the low value of R_f , so that there is little power in the backward propagating field.

Fig. 10 shows the corrected lateral far field profiles measured at different output powers. The corrected far field is obtained as follows. Because of the strong astigmatism, the beam vertically collimated by a spherical lens is convergent in the lateral direction. The corrected far field is obtained by laterally scanning the optical intensity in the beam waist and by calculating the angle as

$$\Theta = \arctan\left(\frac{y}{f}\right), \tag{6}$$

where f is the focal length of the lens [5]. It can be also shown that the corrected far field is exactly the same as the intensity profile that would be found a focal length beyond the measurement lens if an ideal thin cylindrical lens had been placed at the output facet to collimate the beam in the lateral planes removing the quadratic phase curvature due to the divergence of the beam. Fig. 11 shows the uncorrected far field distribution obtained by using a high aperture lens combination, which converts the angular distribution of the divergent beam into a spatial distribution at the plane of a moving slit [9].

The relative power contained in the central lobe of the corrected far field profile is one measure for the beam quality of the tapered laser. As indicated in Fig. 10, even at $P = 3$ W, 80% of the power lies inside the central lobe. The FWHM is 0.25° and the beam propagation ratio is $M_y^2 = 1.1$, calculated from the $1/e^2$ widths of the measured intensity profiles of the uncorrected far field and in the beam waist using Eq. (2). If instead the widths determined with the method of second moments are used, a larger value of M_y^2 is obtained (5.7). One reason is that, in this case, not only the main lobe of the field profile in the beam waist is considered, but also the side lobes, which contain up to 20% of the power (see Fig. 10).

One parameter which has to be carefully optimised is the length L_{RW} of the RW region. Fig. 12 shows the beam propagation ratio M_y^2 versus L_{RW} for a 2 mm long device with a full taper angle of $\varphi = 4^\circ$ and $R_f = 1\%$. Clearly, a minimum of M_y^2 is observed between L_{RW} of 750 and 1000 μm . This minimum is due to a minimum of the width of the intensity profile in the beam waist, whereas the far field angle is nearly constant for $L_{RW} \leq 1000$ μm and decreases above this value [56]. What might be the physical reason for this behaviour of M_y^2 ? If L_{RW} is too short, then higher order modes which are excited in the tapered region and propagate backwards into the RW region are not completely damped and can be reflected at the rear facet back to the RW and tapered regions. This could be possibly prevented by introducing cavity-spoiling grooves or by reducing R_f as simulations reveal [47,48]. Moreover, the power injected into the tapered section rises if L_{RW} is increased and the saturation of

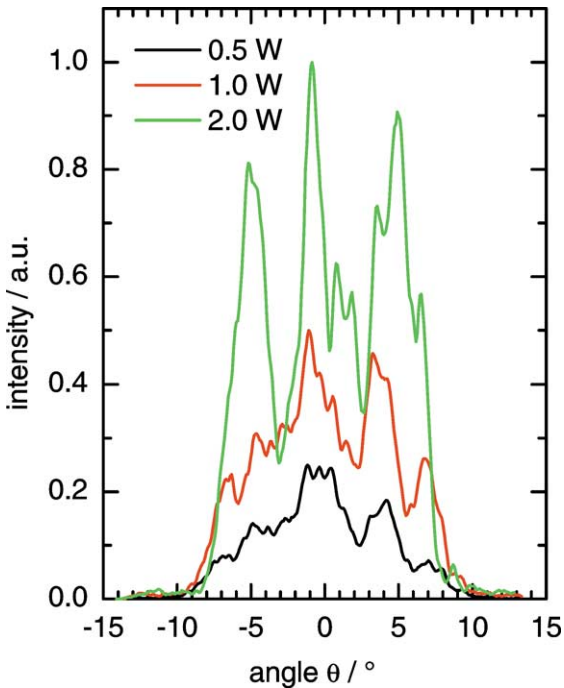


Fig. 11. Profile of the uncorrected lateral far field intensity at the output facet at different output powers for the same device as in Figs. 9 and 10.

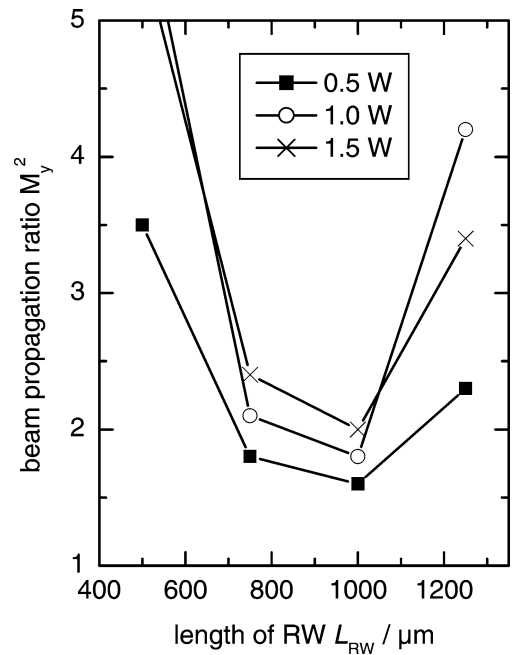


Fig. 12. Beam propagation ratio versus the length of the RW region at different output powers of a 732 nm tapered laser with the following parameters: $L = 2$ mm, $W_{RW} = 3$ μm , $\varphi = 4^\circ$, $R_f = 1\%$.

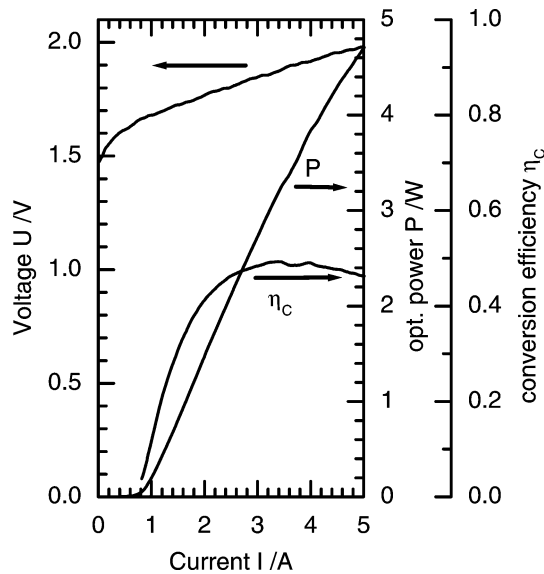


Fig. 13. CW voltage-power-current characteristics of a 808 nm tapered laser with the following parameters: $L = 2.75$ mm, $L_{RW} = 1$ mm, $W_{RW} = 3$ μm , $\varphi = 6^\circ$, $R_f = 0.1\%$. The heatsink temperature was $T = 25^\circ\text{C}$.

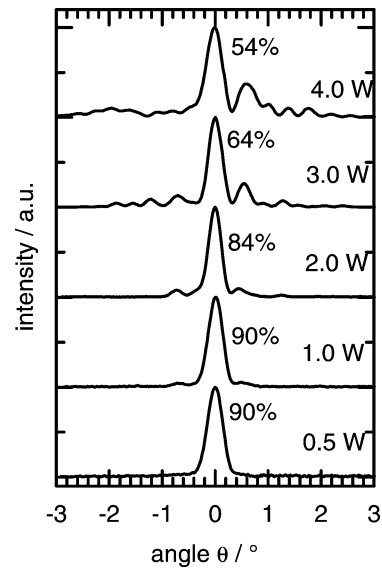


Fig. 14. Profile of the corrected lateral far field intensity at different output powers of a 808 nm tapered laser with the same parameters as in Fig. 13. The relative power in the central lobe is also indicated. The heatsink temperature was $T = 25^\circ\text{C}$.

the gain in the tapered section is more complete, which leads to improved beam stability due to the suppression of the amplified spontaneous emission. However, if L_{RW} becomes too large, a self-focusing effect in the tapered section occurs, and the device tends to oscillate in undesired Fabry–Perot cavity modes, i.e., modes with wavefronts parallel to the facets. This leads again to an increase of M_y^2 .

Finally, we will present results for the 808-nm emitting devices with $L = 2.75$ mm, $\varphi = 6^\circ$, $L_{RW} = 1$ mm, $W_{RW} = 3$ μm , $R_f = 0.1\%$ and effective-index step of $\Delta n_{\text{eff}} = 10^{-2}$. The power-voltage-current characteristics is depicted in Fig. 13. The threshold current is below 0.8 A. For powers up to $P = 3$ W, the slope efficiency is as high as 1.2 W/A and the conversion efficiency is about 50%. The maximum output power (limited by the electrical power supply) is larger than 4.6 W. The corrected lateral far field profiles are depicted in Fig. 14. For powers up to $P = 2$ W, more than 80% of the power lies inside the central lobe. The FWHM is about 0.28° and $M_y^2 = 1.2$ as calculated from the $1/e^2$ widths (3.7 using the method of second moments). At $P = 4$ W, only 54% of the power lies inside the central lobe and $M_y^2 = 3.1$ (10.7).

6. Conclusions

Tapered gain-region devices increase the available output power with high beam quality from semiconductor lasers to the range of about 3 W. The technology is based on well-established single step epitaxy and processing of ridge-waveguide and broad-area devices. The design must be carefully optimised to avoid non-linear distortions of the beam and to achieve a high wall plug efficiency. Due to the low facet load, a very high reliability can be expected. The limits up to now are the decreasing beam quality at high output powers and the low efficiency compared to simple broad area devices.

Despite nearly 15 years work on tapered lasers, further improvements are possible. Nearly all design and technological aspects can be revised in order to achieve higher brightness. These aspects include new vertical structure designs for longer lasers, better mode filtering and improvement of facet stability as the most promising measures. From the physical point of view, there are no fundamental limits to increase the diffraction limited output power to beyond 10 W.

Acknowledgements

The authors thank A. Knauer and F. Bugge for the epitaxy, A. Knigge and J. Fricke for the processing, W. Pittroff for the mounting, R. Staske and F. Dittmar for the measurements of the tapered lasers and E. Larkins (University Nottingham) for

a critical reading of the manuscript. Parts of this work have been funded by the European Community through the research project ULTRABRIGHT (IST-1999-10356) and by the German “Ministerium für Forschung und Technologie” through the research project MDS (13N7371/7).

References

- [1] G.P. Agrawal, *Fiber-Optic Communication Systems*, Wiley, New York, 1997.
- [2] P. Günter (Ed.), *Nonlinear Optical Effects and Materials*, Series in Optical Sciences, Vol. 72, Springer, Berlin, 2000.
- [3] IEEE J. Select. Topics Quantum Electron. 6 (2001), Special Issue on Lasers in Medicine and Biology.
- [4] W. Schulz, R. Poprawe, Manufacturing with novel high-power diode lasers, IEEE J. Select. Topics Quantum Electron. 6 (2000) 696–705.
- [5] J.N. Walpole, Semiconductor amplifiers and lasers with tapered gain regions, Opt. Quantum Electron. 28 (1996) 623–645.
- [6] A.E. Siegmann, New developments in laser resonators, Proc. SPIE 1224 (1990) 2–14.
- [7] International Organization of Standardization, ISO11146.
- [8] D. Botez, Design considerations and analytical approximations for high continuous-wave power, broad-waveguide diode lasers, Appl. Phys. Lett. 74 (1999) 3102–3104.
- [9] R. Hülsewede, J. Sebastian, H. Wenzel, G. Beister, A. Knauer, G. Erbert, Beam quality of high power 800 nm broad-area laser diodes with 1 and 2 μm long optical cavity structures, Opt. Commun. 192 (2001) 69–75.
- [10] E. Kintzer, J.N. Walpole, S.R. Chinn, C.A. Wang, L.J. Missagia, High-power, strained-layer amplifiers and lasers with tapered gain regions, IEEE Photon. Techn. Lett. 5 (1993) 605–608.
- [11] D. Mehuys, L. Goldberg, R. Waarts, D.F. Welch, 4.5 W CW near-diffraction-limited tapered-stripe semiconductor optical amplifier, Electron. Lett. 29 (1993) 219–221.
- [12] S. O’Brien, A. Schönfelder, R.J. Lang, 5-W CW diffraction-limited InGaAs broad-area flared amplifier at 970 nm, IEEE Photon. Techn. Lett. 9 (1997) 1217–1219.
- [13] R. Parke, D.F. Welch, S. O’Brien, R.J. Lang, High power monolithically integrated master-oscillator power amplifiers, presented at the Conf. Lasers and Electro-Optics (CLEO), Baltimore, USA, 1993, paper CTuI4.
- [14] S. O’Brien, D.F. Welch, R. Parke, D. Mehuys, K. Dzurko, R.J. Lang, R. Waarts, D. Scifres, Operating characteristics of a high-power monolithically-integrated flared amplifier master oscillator power amplifier, IEEE J. Quantum Electron. 29 (1993) 2052–2057.
- [15] S. O’Brien, R.J. Lang, R. Parke, J. Major, D.F. Welch, D. Mehuys, 2.2-W continuous-wave, diffraction-limited monolithically integrated master oscillator power amplifier at 854 nm, IEEE Photon. Techn. Lett. 9 (1997) 440–442.
- [16] A. Egan, C.Z. Ning, J.V. Moloney, R.A. Indik, M.W. Wright, D.J. Bossert, J.G. McInerney, Dynamic instabilities in master oscillator power amplifier semiconductor lasers, IEEE J. Quantum Electron. 34 (1998) 166–170.
- [17] G.C. Dente, M.L. Tilton, Modeling multiple-longitudinal-mode dynamics in semiconductor lasers, IEEE J. Quantum Electron. 34 (1998) 325–335.
- [18] R. Lang, K. Kobayashi, External optical feedback effects on semiconductor injection laser properties, IEEE J. Quantum Electron. 16 (1980) 347–355.
- [19] D. Mehuys, S. O’Brien, R.J. Lang, A. Hardy, D.F. Welch, 5W, diffraction-limited, tapered-stripe unstable resonator semiconductor laser, Electron. Lett. 30 (1994) 1855–1856.
- [20] J.N. Walpole, J.P. Donnelly, S.H. Groves, L.J. Missagia, J.D. Woodhouse, R.J. Bailey, A. Napoleone, Diffraction-limited 1.3- μm -wavelength tapered-gain-region lasers with >1-W CW output power, Techn. Lett. 8 (1996) 1429–1431.
- [21] J.P. Donnelly, J.N. Walpole, S.H. Groves, R.J. Bailey, L.J. Missaggia, A. Napoleone, R.E. Reeder, C.C. Cook, 1.5- μm tapered-gain-region lasers with high-CW output powers, IEEE Photon. Techn. Lett. 10 (1998) 1377–1379.
- [22] M. Mikulla, P. Chazan, A. Schmitt, S. Morgott, A. Wetzel, M. Walther, R. Kiefer, W. Pletschen, J. Braunstein, G. Weimann, High-brightness tapered semiconductor laser oscillators and amplifiers with low-modal gain epitaxial structures, IEEE Photon. Techn. Lett. 10 (1998) 654–656.
- [23] S. Delépine, F. Gérard, A. Pinquier, T. Fillion, J. Pasquier, D. Locatelli, J.P. Chardon, H.K. Bissessur, N. Bouché, F.R. Boubal, P. Salet, How to launch 1 W into single-mode fiber from a single 1.48 μm flared resonator, IEEE J. Select. Topics Quantum Electron. 7 (2001) 111–123.
- [24] M.T. Kelemen, F. Rinner, J. Rogg, N. Wiedmann, R. Kiefer, M. Walter, M. Mikulla, G. Weimann, High-power high-brightness ridge-waveguide tapered diode lasers at 940 nm, Proc. SPIE 2648 (2002) 75–81.
- [25] B. Sumpf, R. Hülsewede, G. Erbert, C. Dzionk, J. Fricke, A. Knauer, W. Pittroff, P. Ressel, J. Sebastian, H. Wenzel, G. Tränkle, High-brightness 735-nm tapered diode lasers, Electron. Lett. 38 (2002) 183–184.
- [26] G. Erbert, J. Fricke, R. Hülsewede, A. Knauer, W. Pittroff, P. Ressel, J. Sebastian, B. Sumpf, H. Wenzel, G. Tränkle, 3-W high brightness tapered diode lasers at 735 nm based on tensile-strained GaAsP QWs, Proc. SPIE 4995 (2003).
- [27] M.M. Krakowski, M. Calligaro, S. Auzanneau, F. Berlie, Y. Robert, O. Parillaud, B. Boulant, T. Fillardet, High power and high brightness laser diode structures using Al-free materials, Proc. SPIE 4995 (2003).
- [28] V.V. Wong, S.D. DeMaars, A. Schönfelder, R. Lang, Angled-grating distributed-feedback laser with 1.2 W single-mode diffraction limited output at a 1.06 μm , presented at the Conf. Lasers and Electro-Optics (CLEO) San Francisco, USA, 1998, Technical Digest, pp. 34–35.
- [29] S.D. DeMaars, A. Schönfelder, V. Wong, R.J. Lang, Optical properties of angled-grating distributed feedback lasers, presented at the IEEE Internat. Semiconductor Laser Conference, Nara, Japan, 1998, Digest, pp. 57–58.

- [30] K. Paschke, R. Güther, J. Fricke, J. Sebastian, H. Wenzel, G. Erbert, G. Tränkle, A.P. Bogatov, A.E. Drakin, A.A. Strattonnikov, Design, fabrication and characterization of high-power angled-grating distributed lasers, presented at the IEEE Internat. Semiconductor Laser Conference, Garmisch-Partenkirchen, Germany, 2002, Digest, pp. 16–25.
- [31] K. Paschke, R. Güther, J. Fricke, F. Bugge, G. Erbert, G. Tränkle, High spectral brightness α -DFB lasers in the power range until 3 W at 1060 nm, *Electron. Lett.* (2003), accepted.
- [32] K. Paschke, A. Bogatov, A. Drakin, R. Güther, A. Strattonnikov, H. Wenzel, G. Erbert, G. Tränkle, Modeling and measurements of the radiative characteristics of high-power α -DFB lasers, *IEEE J. Select. Topics Quantum Electron.*, Special Issue on Numerical Simulation of Optoelectronic Devices, 2003, accepted.
- [33] New Series of Landolt–Börnstein, Numerical Data and Functional Relationships in Science and Technology, Springer, Berlin.
- [34] Datareviews Series of Electronic Materials Information Service, INSPEC, London.
- [35] J. Piprek, Semiconductor Optoelectronic Devices – Introduction to Physics and Simulation, Academic Press/Elsevier, Amsterdam, 2002.
- [36] H. Wenzel, H.-J. Wünsche, A model for the calculation of the threshold current of SCH-MQW-SAS lasers, *Phys. Status Solidi A* 120 (1990) 551–673.
- [37] H. Wenzel, G. Erbert, P. Enders, Improved theory of the refractive-index change in quantum-well lasers, *IEEE J. Select. Top. Quantum Electron.* 5 (1999) 637–642.
- [38] H. Wenzel, G. Erbert, F. Bugge, A. Knauer, J. Maegi, J. Sebastian, R. Staske, K. Vogel, G. Tränkle, Optimization of GaAsP-QWs for high-power diode lasers at 800 nm, *Proc. SPIE* 3947 (2000) 32–38.
- [39] G.C. Dente, Low confinement factors for suppressed filaments in semiconductor lasers, *IEEE J. Quantum Electron.* 37 (2001) 1650–1653.
- [40] A. Oster, G. Erbert, H. Wenzel, Gain spectra measurements by a variable stripe length method with current injection, *Electron. Lett.* 33 (1997) 864–865.
- [41] H. Wenzel, G. Erbert, Simulation of single-mode high-power semiconductor lasers, *Proc. SPIE* 2693 (1996) 418–429.
- [42] Available online: <http://www-ocs.colorado.edu/SimWindows/simwin.html>.
- [43] H.-J. Wünsche, U. Bandelow, H. Wenzel, Calculation of combined lateral and longitudinal spatial hole burning in $\lambda/4$ shifted DFB lasers, *IEEE J. Quantum Electron.* 29 (1993) 1751–1760.
- [44] M. Niederhoff, Feldberechnung in Hochleistungslaserdioden, Ph.D. Thesis, München, 1996.
- [45] J. Wykes, L. Borruel, S. Sujecki, I. Esquivias, P. Sewell, T.M. Benson, E.C. Larkins, P. Moreno, M. Krakowski, Hot-cavity modelling of high-power tapered laser diodes using wide-angle 3D FD-BPM, in: *IEEE/LEOS Annual Meeting, Conference Proceedings*, 2002, pp. 91–92.
- [46] L. Borruel, S. Sujecki, I. Esquivias, J. Wykes, P. Sewell, T.M. Benson, E.C. Larkins, J. Arias, B. Romero, A selfconsistent electrical, thermal and optical model of high brightness tapered lasers, *Proc. SPIE* 4646 (2002) 355–366.
- [47] S. Sujecki, L. Borruel, J. Wykes, P. Moreno, B. Sumpf, P. Sewell, H. Wenzel, T.M. Benson, G. Erbert, I. Esquivias, E.C. Larkins, Nonlinear properties of tapered laser cavities, *IEEE J. Select. Topics Quantum Electron.*, Special Issue on Numerical Simulation of Optoelectronic Devices (2003), submitted.
- [48] S. Mariojouis, S. Margott, A. Schmitt, M. Mikulla, J. Braunstein, G. Weimann, F. Lozes, S. Bonenfant, Modeling of the performance of high-brightness tapered lasers, *Proc. SPIE* 3944 (2000) 395–406.
- [49] K.H. Hasler, H. Wenzel, A. Klehr, G. Erbert, Simulation of the generation of high-power pulses in the GHz range with three-section DBR lasers, *IEE Proc. Optoelectron.* 149 (2002) 152–160.
- [50] E. Gehrig, O. Hess, R. Wallenstein, Modeling of the performance of high-power diode amplifier systems with an optothermal microscopic spatio-temporal theory, *IEEE J. Quantum Electron.* 35 (1999) 320–331.
- [51] R. Diehl (Ed.), High-Power Diode Lasers, Topics in Applied Physics, Vol. 78, Springer, Berlin, 2000.
- [52] A. Knauer, H. Wenzel, G. Erbert, B. Sumpf, W. Weyers, Influence of oxygen in AlGaAs-based laser structures with Al-free active region on device properties, *J. Electron. Mater.* 30 (2001) 1421–1424.
- [53] W. Pittroff, G. Erbert, G. Beister, F. Bugge, A. Klein, A. Knauer, J. Maegi, P. Ressel, J. Sebastian, R. Staske, G. Tränkle, Mounting of high power laser diodes on boron nitride heat sinks using an optimized Au/Sn metallurgy, *IEEE Trans. Adv. Packaging* 24 (2001) 434–441.
- [54] O. Ceburkov, H. Gollnick, Photodynamic therapy in dermatology, *Eur. J. Dermatol.* 10 (2000) 567–568.
- [55] G. Erbert, F. Bugge, A. Knauer, J. Sebastian, A. Thies, H. Wenzel, M. Meyers, G. Tränkle, *J. Select. Top. Quantum Electron.* 5 (1999) 780–784.
- [56] B. Sumpf, R. Hülsewede, G. Erbert, C. Dzionk, J. Fricke, A. Knauer, W. Pittroff, P. Ressel, J. Sebastian, G. Tränkle, High brightness 735 nm tapered lasers – optimisation of the laser geometry, *Optical and Quantum Electronics* 35 (2003) 521–532.